Optical properties of zinc-blende semiconductor alloys: Effects of epitaxial strain and atomic ordering

Su-Huai Wei and Alex Zunger
National Renewable Energy Laboratory, Golden, Colorado 80401
(Received 1 November 1993)

Spontaneous ordering of III-V alloys is known to cause a band-gap reduction $|\Delta E_g|$ and a splitting ΔE_{12} of the valence-band maximum. Strain also leads to a valence-band splitting and, depending on the sign of the strain ϵ, to an increase (for $\epsilon < 0$) or decrease (for $\epsilon > 0$) in the band gap. We present a general theory explaining how the strain produced by lattice mismatch with the substrate interacts with ordering effects. We find for (001) strain and (111) "CuPt" ordering that (i) atomic ordering removes the cusp in the band gap vs strain curve of random alloys; (ii) epitaxial strain always leads to an *increase* in the ordering-induced valence-band splitting ΔE_{12}; (iii) atomic ordering *reduces* the slope of ΔE_{12} vs strain; and (iv) while (a) strain; (b) ordering, and (c) clustering can all lead to a band-gap reduction, we show here that the three effects can be partially distinguished on the basis of a ΔE_{12} vs $|\Delta E_g|$ plot; and (v) the wave-function type at the valence-band maximum (VBM) (and, hence, the cause of the splitting) can be further determined by measuring the polarization dependence of the *intensities* of the transitions between the VBM split components and the conduction-band minimum; (vi) we predict that ordering can significantly enhance the degree of spin polarization of photoelectrons emitted from the VBM. Ordered III-V alloys can thus be used as a good polarized electron source. These general results open new avenues of band-gap engineering by combining epitaxial strain with atomic ordering. Specific experimentally testable predictions are presented.

I. INTRODUCTION

At threshold, the optical properties of direct-band-gap zinc-blende semiconductors are determined by (including the spin-orbit interactions) the $\Gamma_{8v} \longleftrightarrow \Gamma_{6c}$ transitions. These transitions can be split into heavy-hole and light-hole components by applying *external* fields, e.g., strain,[1–29] or by *internal* field, e.g., atomic (superlattice) ordering.[30,31] Most theoretical works on these threshold transitions considered the first case, focusing on how strain splits the Γ_{8v} states at the valence-band maximum (VBM) and changes the band-gap energy.[1–19] Experiments on strain effects in cubic zinc-blende semiconductors[4,6–8] and on their cubic random alloys [$Ga_xIn_{1-x}P$,[20–25] $Ga_xIn_{1-x}As$,[21,26,27] or SiGe (Refs. 28 and 29)] have indeed confirmed that the VBM splits almost linearly with strain, and that the band gap vs strain curve changes slope as the strain changes from compressive to tensile.[20–25] Here, we consider the interesting case where the film is atomically ordered, so its Γ_{8v} state is already split by the lower symmetry of the ordering potential even without strain. Application of strain then leads to interesting and unexpected results.

Atomic ordering corresponds to a periodic arrangement of atomic planes along a given crystal axis $\mathbf{G}_{\text{ord}}$. Examples include (i) Spontaneous CuPt ordering observed in homogeneous vapor-phase growth of virtually all III-V alloys,[30] yielding alternate monolayer superlattices along $\mathbf{G}_{\text{ord}} = [111]$. This leads to significant predicted[32–34] and observed[35,36] $\Gamma_{4v,5v}$-Γ_{6v} splitting at the VBM. (ii) Artificially grown $\mathbf{G}_{\text{ord}} = [001]$ superlattices have been predicted[32,37,38] to have Γ_{6v}-Γ_{7v} splittings at the VBM. In conventional strained layer superlattices the direction $\mathbf{G}_{\text{ord}}$ of layer modulations coincides, by choice, with the substrate orientation $\mathbf{G}_{\text{substrate}}$, so the effects of atomic ordering and strain add up colinearly. In contrast, spontaneously ordered systems often exibit ordering along $\mathbf{G}_{\text{ord}} \neq \mathbf{G}_{\text{substrate}}$. This leads to the interesting case where a semiconductor is subjected to noncolinear "chemical strain" along $\mathbf{G}_{\text{ord}}$ and to "elastic strain" along $\mathbf{G}_{\text{substrate}}$. We study here the consequence of such "double strain" on the optical properties at threshold. We give easy-to-use expressions for the separate effects of $\mathbf{G}_{\text{ord}}$ or $\mathbf{G}_{\text{strain}}$ on the valence and conduction bands. We then show how the existence of "double strain" changes the optical properties relative to the pure epitaxial strain or pure ordering cases. Most distinctively, for atomic ordering along [111] and epitaxial strain along [001]: (i) Atomic ordering is shown to remove the "cusp" in the band gap vs strain curve of random alloy.[20,21,23–25] (ii) Epitaxial strain always leads to an *increase* in the ordering-induced valence-band splitting ΔE_{12}, and (iii) atomic ordering *reduces* the slope of ΔE_{12} vs strain. (iv) While (a) strain, (b) ordering, and (c) clustering can all lead to a band-gap reduction, we show here that the three effects can be distinguished on the basis of a ΔE_{12} vs $|\Delta E_g|$ plot. (v) The wave-function type, and, hence, the cause of the splitting at the VBM can be determined by measuring the polarization-dependent *intensities* of the transitions between the split components of the valence band and the conduction-band minimum.

(vi) We predict that ordering can significantly enhance the degree of spin polarization of electrons photoemitted from the VBM. Ordered III-V alloys can thus be used as a good polarized electron source. These general results open avenues of band-gap engineering by combining epitaxial strain with atomic ordering. Experimentally testable predictions are made and summarized in Sec. IV.

II. EFFECTS OF STRAIN AND ORDERING ON Γ POINT STATES

We will characterize the quantities of interest in terms of the degree of long range order η and the strain ϵ. Our reference state is a perfectly random ($\eta = 0$), strain-free ($\epsilon = 0$) system. In this case, and in the absence of spin-orbit coupling the top of the $\mathbf{k} = 0$ valence band is the sixfold degenerate Γ_{15v} state while the bottom of the conduction band is the Γ_{1c} doublet. The degeneracy at the valence-band edge can be lifted by spin-orbit coupling, epitaxial strain, or by alloy atomic ordering. We denote as Δ^S and Δ^O the strain-(S-) induced and the ordering- (O-) induced crystal field splitting, respectively, and by $\Delta^{\rm SO}$ the spin-orbit (SO) splitting. In the following we will develop a general formula to describe the combined effects of epitaxial strain, atomic ordering, and spin-orbit coupling on the band edge energy levels. We will first discuss each individual term, and then assume additivity, i.e., the total effects can be described by $H^S + H^O + H^{\rm SO}$.

A. Pure elastic strain

The effects of epitaxial strain on the energy levels have been studied quite extensively by a number of authors.[1–19] A review of strain effects on electronic properties of semiconductors can be found in Ref. 4 and Ref. 8. In Ref. 4 Pollak and Cardona derived explicitly the expressions for the strain Hamiltonian in the (J, m_J) momentum representation for strain along the [001], [111], and [110] directions. In the following we will derive an explicit general expression of the strain Hamiltonian in the (x, y, z) Cartesian representation. This representation is more convenient in describing the coupling between strain, atomic ordering, and spin-orbit effects.

When a cubic lattice is deformed, a position $\mathbf{r} = (x, y, z)$ in the lattice is displaced to a position $\mathbf{r}' = (x', y', z')$. To linear order, the displacement $\Delta\mathbf{r} = \mathbf{r}' - \mathbf{r}$ is given by

$$\Delta\mathbf{r} = (x\epsilon_{xx} + y\epsilon_{yx} + z\epsilon_{zx}, x\epsilon_{xy} + y\epsilon_{yy} + z\epsilon_{zy}, x\epsilon_{xz} + y\epsilon_{yz} + z\epsilon_{zz}) , \tag{1}$$

where $\epsilon_{\mu\nu}$ are the components of the strain tensor. For an epitaxial strain along the direction $\mathbf{G} = [l, m, n]$, the strain tensor is given by

$$\overleftrightarrow{\epsilon} = \delta \begin{pmatrix} l^2 + \epsilon_0 & lm & ln \\ lm & m^2 + \epsilon_0 & mn \\ ln & mn & n^2 + \epsilon_0 \end{pmatrix} , \tag{2}$$

where ϵ_0 is a constant describing hydrostatic deformation and δ is a scale factor.

Based on symmetry considerations and the assumption of linearity, the strain Hamiltonian H_j^S for the jth band at $\mathbf{k} = 0$ can be written as[1–4]

$$H_j^S = a_j(\epsilon_{xx} + \epsilon_{yy} + \epsilon_{zz}) - 3b_j[(L_x^2 - \tfrac{1}{3}\mathbf{L}^2)\epsilon_{xx} + \text{c.p.}]$$
$$-(6d_j/\sqrt{3})[\{L_x, L_y\}\epsilon_{xy} + \text{c.p.}] . \tag{3}$$

Here, $\mathbf{L}$ is the angular momentum operator, $\{L_x, L_y\} = \frac{1}{2}(L_xL_y + L_yL_x)$, the coefficient a_j is the hydrostatic deformation potential for band j, while b_j and d_j are uniaxial deformation potentials appropriate to strains of tetragonal and rhombohedral symmetries, respectively. c.p. denotes in Eq. (3) cyclical permutations with respect to the indices x, y, and z. We next specialize Eq. (3) to the $j = \Gamma_1$ and $j = \Gamma_{15}$ states of zinc-blende semiconductors.

For the Γ_{1c} conduction (c) band, Eq. (3) is simplified using the $L = 0$ representation of the angular momentum operator $\mathbf{L} = \mathbf{0}$. This gives

$$H_c^S = a_c(\epsilon_{xx} + \epsilon_{yy} + \epsilon_{zz}) = a_c\frac{\Delta V}{V} , \tag{4}$$

where $\frac{\Delta V}{V} = \epsilon_{xx} + \epsilon_{yy} + \epsilon_{zz}$ is the relative volume deformation. For the Γ_{15v} states at the top of the valence (v) band we can rewrite Eq. (3) using the $L = 1$ matrix representation[39] of the angular momentum operator

$$L_x = \begin{pmatrix} 0 & 0 & 0 \\ 0 & 0 & -i \\ 0 & i & 0 \end{pmatrix}; \quad L_y = \begin{pmatrix} 0 & 0 & i \\ 0 & 0 & 0 \\ -i & 0 & 0 \end{pmatrix}; \tag{5}$$
$$L_z = \begin{pmatrix} 0 & -i & 0 \\ i & 0 & 0 \\ 0 & 0 & 0 \end{pmatrix},$$

where $i = \sqrt{-1}$. This gives

$$H_v^S = a_v \frac{\Delta V}{V} - b_v \left[\begin{pmatrix} -2 & 0 & 0 \\ 0 & 1 & 0 \\ 0 & 0 & 1 \end{pmatrix} \epsilon_{xx} + \begin{pmatrix} 1 & 0 & 0 \\ 0 & -2 & 0 \\ 0 & 0 & 1 \end{pmatrix} \epsilon_{yy} + \begin{pmatrix} 1 & 0 & 0 \\ 0 & 1 & 0 \\ 0 & 0 & -2 \end{pmatrix} \epsilon_{zz} \right]$$
$$-\sqrt{3} d_v \left[\begin{pmatrix} 0 & -1 & 0 \\ -1 & 0 & 0 \\ 0 & 0 & 0 \end{pmatrix} \epsilon_{xy} + \begin{pmatrix} 0 & 0 & 0 \\ 0 & 0 & -1 \\ 0 & -1 & 0 \end{pmatrix} \epsilon_{yz} + \begin{pmatrix} 0 & 0 & -1 \\ 0 & 0 & 0 \\ -1 & 0 & 0 \end{pmatrix} \epsilon_{zx} \right] . \quad (6)$$

The solutions of H_v^S give three energy levels, E_1, E_2, and E_3 for each strain. As will be illustrated next, this Hamiltonian can be further simplified for strain parallel to the high symmetry [001] or [111] directions.

For (001) strain we have from Eq. (2) $\epsilon_{xx} = \epsilon_{yy} \neq \epsilon_{zz}$ and $\epsilon_{xy} = \epsilon_{yz} = \epsilon_{zx} = 0$, so the third term in Eq. (6) vanishes. The Hamiltonian becomes[8]

$$H_{001,v}^S = a_v \frac{\Delta V}{V} + \frac{1}{3} \Delta_{001}^S(\epsilon) \begin{pmatrix} 1 & 0 & 0 \\ 0 & 1 & 0 \\ 0 & 0 & -2 \end{pmatrix} . \quad (7)$$

In this case E_1 and E_2 are degenerate, while E_3 is separated from E_1 and E_2 by the crystal field splitting $\Delta_{001}^S(\epsilon)$, which is given by

$$\Delta_{001}^S = -3 b_v [\epsilon_{zz} - \epsilon_{xx}] . \quad (8)$$

For (111) strain we have from Eq. (2) $\epsilon_{xx} = \epsilon_{yy} = \epsilon_{zz}$ and $\epsilon_{xy} = \epsilon_{yz} = \epsilon_{zx}$, so the second term in Eq. (6) vanishes, and the Hamiltonian becomes[8]

$$H_{111,v}^S = a_v \frac{\Delta V}{V} + \frac{1}{3} \Delta_{111}^S(\epsilon) \begin{pmatrix} 0 & -1 & -1 \\ -1 & 0 & -1 \\ -1 & -1 & 0 \end{pmatrix} . \quad (9)$$

Again, in this case E_1 and E_2 are degenerate while E_3 is separated from E_1 and E_2 by the crystal field splitting $\Delta_{111}^S(\epsilon)$, which is given by

$$\Delta_{111}^S = -3\sqrt{3} d_v \epsilon_{xy} . \quad (10)$$

[In our notation, $\Delta_{\mathbf{G}}$ is positive if the doublet eigenvalues of Eqs. (7) and (9) lie *above* the singlet.] Note that $H_{111,v}^S$ can be brought to the same form as $H_{001,v}^S$ by applying a unitary transformation, rotating the [111] direction to coincide with the z axis. For all other directions the tetragonal and rhombohedral deformation potential are coupled to each other[4] and no degeneracy exists except when $b_v = d_v/\sqrt{3}$. In this special case the band splitting becomes isotropic, thus, for any epitaxial strain along $\mathbf{G}$ we can find a unitary transformation which rotates the z axis to coincide with the $\mathbf{G}$ direction, so the Hamiltonian of Eq. (6) acquires the same form as $H_{001,v}^S$ in Eq. (7).

Since only *relative* energy differences between two bands are generally measured, it will be convenient to define the center of the valence-band energy as our zero of energy and denote by $a = a_c - a_v$ the deformation potential of the average band gap $\bar{E}_g = E_c - \frac{1}{3}(E_1 + E_2 + E_3)$. From now on we will also drop the band index j for the deformation parameters b and d, since they are used only for the top of the valence band.

B. Pure atomic ordering

It is now known[30] that vapor-phase growth of most III-V zinc-blende semiconductor alloys results in spontaneously ordered structures. Most of these ordered structures can be characterized as superlattices. For example, the ordered CuPt-like structure is an alternate monolayer superlattice along the $\mathbf{G}_{\text{ord}} = [111]$ direction, while the ordered CuAuI-like structure is an alternate monolayer superlattice along the $\mathbf{G}_{\text{ord}} = [001]$ direction. This atomic ordering is analogous to an "internal strain" in that the ordering changes the band-gap energy and the splitting at the top of the valence bands in the same way as external elastic strain. The Hamiltonian used to describe the energy level shift due to the atomic ordering along $\mathbf{G}_{\text{ord}}$ has the same form [Eqs. (3)] as the one used to describe epitaxial strain along $\mathbf{G}_{\text{ord}}$, except that, for long range atomic order, the fictitious internal strain "$\epsilon_{\mu,\nu}$" and deformation potentials a, b, and d are functions of the ordering vector $\mathbf{G}_{\text{ord}}$ and the order parameter η.

For example, for the widely observed CuPt-like ordering,[30] the Hamiltonian which describes the valence-band splitting due to atomic ordering can be obtained by replacing $\Delta_{111}^S(\epsilon)$ in Eq. (9) by $\Delta_{111}^O(\eta)$, i.e.,

$$H_{111,v}^O = \frac{1}{3} \Delta_{111}^O(\eta) \begin{pmatrix} 0 & -1 & -1 \\ -1 & 0 & -1 \\ -1 & -1 & 0 \end{pmatrix} , \quad (11)$$

where $\Delta_{111}^O(\eta)$ is the crystal field splitting due to the atomic ordering. For *perfect* long range order ($\eta = 1$), the crystal field splitting can be calculated from band theory. This was done for CuPt ordering[32,33] ($\mathbf{G}_{\text{ord}} = [111]$) and for CuAu ordering[32,37,38] ($\mathbf{G}_{\text{ord}} = [001]$). Similar calculations have been done for chalcopyrite ordering[32,40] ($\mathbf{G}_{\text{ord}} = [201]$), assuming a higher symmetry, tetragonal unit cell. We found that[32] for isovalent alloys, because of the different band folding relations, $\Delta_{111}^O > \Delta_{001}^O > \Delta_{201}^O$. Δ_{111}^O and Δ_{001}^O are positive, while the Δ_{201}^O are mostly negative.

In *imperfectly* ordered $A_x B_{1-x} C$ alloys, successive ordering planes are not pure A and pure B, but $A_{x+\frac{\eta}{2}} B_{1-x-\frac{\eta}{2}}$ and $A_{x-\frac{\eta}{2}} B_{1-x+\frac{\eta}{2}}$, respectively. Wei, Laks, and Zunger[34] showed that for an alloy with a long range order parameter η, any physical properties $P(x,\eta)$ at composition x can be expressed in terms of the properties $P(x,0)$ and $P(X_\sigma,0)$ of the perfectly *random* alloy at composition x and X_σ, and the property $P(X_\sigma,1)$ of the perfectly *ordered* structure σ at composition X_σ:

$$P(x,\eta) = P(x,0) + \eta^2 \left[P(X_\sigma,1) - P(X_\sigma,0)\right] , \quad (12)$$

provided that the property can be well expressed in terms of single-site and pair interactions. Because the crystal field splitting in the absence of ordering ($\eta = 0$) is zero, we have from Eq. (12)

$$\Delta^O_{111}(\eta) = \eta^2 \Delta^O_{111}(\eta = 1) . \quad (13)$$

Note that x and X_σ do not have to be the same. However, since the ordering parameter is limited[34] by

$$0 \le \eta \le \min\left(\frac{x}{X_\sigma}, \frac{1-x}{1-X_\sigma}\right) , \quad (14)$$

perfect ordering can be achieved only when $x = X_\sigma$. Due to the neglect of higher order terms, Eq. (12) assumes that the *change* $P(x,\eta) - P(x,0)$ does not depend on x and can be calculated knowing the quantities at $x = X_\sigma$. This approximation[34] is best when $x \simeq X_\sigma = \frac{1}{2}$.

C. Spin-orbit coupling

The spin-orbit (SO) coupling for the s-like Γ_{1c} state is zero. The spin-orbit coupling Hamiltonian for the spin up ($\uparrow$) and spin down ($\downarrow$) Γ_{15v} states in the Cartesian representation ($x\uparrow, y\uparrow, z\uparrow, x\downarrow, y\downarrow, z\downarrow$) is not block diagonal, so we have to use a full 6×6 matrix to represent the spin-orbit Hamiltonian in this basis,[41] that is

$$H^{\rm SO} = \frac{1}{3}\Delta^{\rm SO} \begin{pmatrix} 0 & -i & 0 & 0 & 0 & 1 \\ i & 0 & 0 & 0 & 0 & -i \\ 0 & 0 & 0 & -1 & i & 0 \\ 0 & 0 & -1 & 0 & i & 0 \\ 0 & 0 & -i & -i & 0 & 0 \\ 1 & i & 0 & 0 & 0 & 0 \end{pmatrix} . \quad (15)$$

Note that the spin-orbit splitting $\Delta^{\rm SO}$ is defined to be positive if the fourfold degenerate eigenvalue of Eq. (15) is above the doublet. We have also chosen the phase factor such that the up spin $\uparrow$ and down spin $\downarrow$ are parallel and antiparallel to the [001] direction, respectively.

D. The total Hamiltonian

In constructing the total Hamiltonian $H_{\rm tot}$ we make the assumption that the contributions from the elastic strain, the atomic ordering, and the spin-orbit coupling are additive. That is

$$H_{\rm tot} = H_0 + H^S + H^O + H^{\rm SO} , \quad (16)$$

where H_0 is the energy in the absence of strain, ordering, and spin-orbit coupling. Note that strain and ordering do not remove[4] the Kramers (spin) degeneracy of each state at Γ.

Applying Eq. (16) to the Γ_{1c} conduction state, we find that its energy relative to the center of the top valence bands at Γ (our energy zero) is given by

$$E_c(\eta,\epsilon) = E_c(0,0) + a\frac{\Delta V(\epsilon)}{V} + \bar{B}_g\eta^2 . \quad (17)$$

The second term on the right hand side of Eq. (17) is due to hydrostatic strain and a is the hydrastatic band-gap deformation potential. The third term is due to ordering and $\bar{B}_g$ is the *average* band-gap reduction $\Delta\bar{E}_g$ of the strain-free perfectly ordered alloy relative to the strain-free perfectly random alloy.

For the top valence states, the total Hamiltonian of Eq. (16) is a 6×6 matrix: The elastic strain and atomic ordering give each two 3×3 block diagonal matrices where each block has the form given by Eq. (6). The spin-orbit part is a full 6×6 matrix given by Eq. (15). In the next section, we will give two examples of the total Hamiltonian.

In many practical cases we can assume that the mixing of the wave-functions between different states is small,[42] so the parameters associated with each contribution in Eq. (16) can be determined separately. A simple test indicates that these assumptions are reasonable. For example, the spin-orbit splitting $\Delta^{\rm SO}$ of GaAs calculated with strain ($|\epsilon| = 0.4\%$, see below) or without strain differs by less than 1 meV. The spin-orbit splitting $\Delta^{\rm SO}$ of $Ga_{0.5}In_{0.5}P$ calculated with ($\eta = 1$) or without (111) atomic ordering differs by less than 5 meV. In what follows, we assume both additivity [Eq. (16)] and uncoupling of the crystal and spin-orbit splittings.

III. EXAMPLES

A. Pure (001) epitaxial strain

In this section, we consider a cubic zinc-blende film ($\eta = 0$) with equilibrium lattice constant a_f grown coherently on a substrate with a lattice constant a_s and orientation $\mathbf{G}_{\rm substrate} = [l,m,n]$. The biaxial strain $\epsilon_\perp$ perpendicular to the growth direction is given by

$$\epsilon_\perp = \frac{a_s - a_f}{a_f} . \quad (18)$$

Using continuous elasticity theory, the epitaxial strain $\epsilon_\parallel$ parallel to the growth direction is given by[43,44]

$$\epsilon_\parallel = [3q(\mathbf{G}) - 2]\epsilon_\perp . \quad (19)$$

Here, $q(\mathbf{G}) = 1 - B/[C_{11} + \gamma(\mathbf{G})\zeta]$ is the strain reduction factor, $B = (C_{11} + 2C_{12})/3$ is the bulk modulus, $\zeta = C_{44} - (C_{11} - C_{12})/2$ is the elastic anisotropy, C_{ij} are the elastic constants, and the orientation dependence is given by[44] $\gamma(\mathbf{G}) = 4(l^2m^2 + m^2n^2 + n^2l^2)/(l^2 + m^2 + n^2)^2$. Applying these to $\mathbf{G}_{\rm substrate} = [001]$, we have $\epsilon = \epsilon_{xx} = \epsilon_{yy} = \epsilon_\perp$ and

$$\epsilon_{zz} = \epsilon_\parallel = -\frac{2C_{12}}{C_{11}}\epsilon , \quad (20)$$

so

$$\frac{\Delta V(\epsilon)}{V} = 2\frac{C_{11} - C_{12}}{C_{11}}\epsilon . \quad (21)$$

In our definition ϵ is negative (positive) for in-plane compression (tension). From Eq. (17) the conduction-band energy relative to the center of the top valence bands is given by

$$E_c(\epsilon) = E_c(0) + 2a\frac{C_{11}-C_{12}}{C_{11}}\epsilon \ . \tag{22}$$

The Hamiltonian for the top of the valence states can be obtained by combining Eq. (7) with Eq. (15), i.e.,

$$H_v = \frac{1}{3}\begin{pmatrix} \Delta^S_{001} & -i\Delta^{\rm SO} & 0 & 0 & 0 & \Delta^{\rm SO} \\ i\Delta^{\rm SO} & \Delta^S_{001} & 0 & 0 & 0 & -i\Delta^{\rm SO} \\ 0 & 0 & -2\Delta^S_{001} & -\Delta^{\rm SO} & i\Delta^{\rm SO} & 0 \\ 0 & 0 & -\Delta^{\rm SO} & \Delta^S_{001} & i\Delta^{\rm SO} & 0 \\ 0 & 0 & -i\Delta^{\rm SO} & -i\Delta^{\rm SO} & \Delta^S_{001} & 0 \\ \Delta^{\rm SO} & i\Delta^{\rm SO} & 0 & 0 & 0 & -2\Delta^S_{001} \end{pmatrix} , \tag{23}$$

where the crystal field splitting is

$$\Delta^S_{001}(\epsilon) = 3b\frac{C_{11}+2C_{12}}{C_{11}}\epsilon \ . \tag{24}$$

Diagonalization of Eq. (23) gives three spin degenerate eigenvalues of the *in-plane* light-hole (lh) [Γ_{6v}; ($j = 3/2, m_j = \pm 3/2$)], heavy-hole (hh) [Γ_{7v}; ($j = 3/2, m_j = \pm 1/2$)], and spin-orbit split-off (SO) [Γ_{7v}; ($j = 1/2, m_j = \pm 1/2$)] states. Here, we use the notation of Ref. 21. Note that along the [001] direction the roles of light-hole and heavy-hole are reversed. Explicitly,[4,42]

$$\begin{aligned} E^{\rm lh}(\epsilon) &= \frac{1}{3}[\Delta^{\rm SO} + \Delta^S_{001}(\epsilon)] \ , \\ E^{\rm hh}(\epsilon) &= -\frac{1}{6}[\Delta^{\rm SO} + \Delta^S_{001}(\epsilon)] \\ &\quad + \frac{1}{2}\sqrt{[\Delta^{\rm SO} + \Delta^S_{001}(\epsilon)]^2 - \frac{8}{3}\Delta^{\rm SO}\Delta^S_{001}(\epsilon)} \ , \\ E^{\rm SO}(\epsilon) &= -\frac{1}{6}[\Delta^{\rm SO} + \Delta^S_{001}(\epsilon)] \\ &\quad - \frac{1}{2}\sqrt{[\Delta^{\rm SO} + \Delta^S_{001}(\epsilon)]^2 - \frac{8}{3}\Delta^{\rm SO}\Delta^S_{001}(\epsilon)} \ . \end{aligned} \tag{25}$$

For systems with no strain ($\epsilon = 0$) the lh and hh states are the degenerate cubic Γ_{8v} state. Note that the *crystal field splitting* $\Delta^S_{001}(\epsilon)$ does not correspond to a difference of measurable levels. The measurable *valence-band splitting* is given by $|E^{\rm lh} - E^{\rm hh}|$.

Equations (22) and (25) give the the band-edge energies as functions of the (001) strain. To relate the energies above to the measured energy differences (i.e., the band gaps) we will consider the case when the strain ϵ is small and the band gaps change linearly with ϵ. For the light-hole band gap $E^{\rm lh}_g(\epsilon) = E_c(\epsilon) - E^{\rm lh}(\epsilon)$ the strain shift is[21]

$$\Delta E^{\rm lh}_g(\epsilon) \equiv E^{\rm lh}_g(\epsilon) - E^{\rm lh}_g(0) \cong -\alpha\epsilon \ , \tag{26}$$

while for the heavy-hole band gap $E^{\rm hh}_g(\epsilon) = E_c(\epsilon) - E^{\rm hh}(\epsilon)$ the strain shift is[21]

$$\Delta E^{\rm hh}_g(\epsilon) \equiv E^{\rm hh}_g(\epsilon) - E^{\rm hh}_g(0) \cong -\beta\epsilon \ . \tag{27}$$

Using Eqs. (22)–(27) in the linear region we have

$$\begin{aligned} \alpha &= [-2a(C_{11}-C_{12}) + b(C_{11}+2C_{12})]/C_{11} \ , \\ \beta &= [-2a(C_{11}-C_{12}) - b(C_{11}+2C_{12})]/C_{11} \ , \\ \Delta^S_{001}(\epsilon) &= \tfrac{3}{2}(\alpha-\beta)\epsilon \end{aligned} \tag{28}$$

and

$$\begin{aligned} E_c(\epsilon) = E_c(0) - \tfrac{1}{2}(\alpha+\beta)\epsilon &= E_g(0) + \tfrac{1}{3}\Delta^{\rm SO} \\ &\quad - \tfrac{1}{2}(\alpha+\beta)\epsilon \ , \end{aligned} \tag{29}$$

where $E_g(0)$ is the band gap at $\epsilon = 0$ and $E_c(0) = E_g(0) + \frac{1}{3}\Delta^{\rm SO}$ when $\Delta^{\rm SO} > 0$. This is true for all III-V's.[45]

In Table I we list the experimental[45] room tempera-

TABLE I. Experimental parameters used to calculate band edge energy level shifts as functions of strain and ordering. All experimental values are taken at room temperature from Ref. 45. See text for details.

Properties	GaAs	InAs	GaP	InP	$Ga_{0.5}In_{0.5}P$
a_0 (Å)	5.6533	6.0583	5.4512	5.8687	5.6600
E_g (eV)	1.43	0.36	2.78	1.35	1.88
$\Delta^{\rm SO}$ (eV)	0.34	0.37	0.08	0.11	0.10
C_{11} (GPa)	118	83	141	102	122
C_{12} (GPa)	53	45	62	58	60
a (eV)	−9.8	−6.0	−9.9	−6.4	−8.2
b (eV)	−2.0	−1.8	−1.8	−1.6	−1.7
α (eV)	7.0	1.7	7.7	2.1	4.9
$\alpha_{\rm LDA}$ (eV)	3.2	0.5	4.8	0.8	2.8
β (eV)	14.6	9.2	14.5	8.9	11.7
$\beta_{\rm LDA}$ (eV)	11.0	7.6	12.1	7.5	9.8

ture elastic constants C_{ij} and deformation potentials a and b for the III-V semiconductor compounds GaP, InP, GaAs, and InAs. Using Eq. (28) we give also α and β for the four compounds show in Table I. We have also calculated α and β directly from Eqs. (26) and (27) using the first-principles linearized augmented plane wave (LAPW) method[46] within the local density approximation (LDA).[47,48] The calculated $T = 0$ values $\alpha_{\rm LDA}$ and $\beta_{\rm LDA}$ are given in Table I. We find that the calculated LDA values are systematically smaller than the experimental values measured at room temperature. This could be due to the strong temperature dependence of the band-gap deformation potential. For example, for GaAs,[49] a at $T = 120$ K is about 3 eV smaller than at room temperature. This, in turn, will reduce α and β by the same magnitude [Eq. (28)]. However, the calculated difference $\alpha_{\rm LDA} - \beta_{\rm LDA}$, which determines the valence-band splitting, agrees very well with experimental data.

Using the room temperature experimental data given in Table I, we plot in Fig. 1 the $E^{\rm lh}, E^{\rm hh}, E^{\rm SO}$, and E_c energy levels of GaAs using Eq. (25) and Eq. (29). These are individual energy levels (not gaps), taken with respect to the center of the top valence bands. Figure 2 shows the band gap $E_g(\epsilon) = E_c(\epsilon) - E_{\rm VBM}(\epsilon)$ as a function of strain. We find the following

(i) For in-plane compressive stress $\epsilon < 0$ (i.e., $a_s < a_0$) the top of the valence band is the in-plane light-hole state.[21,16] This may enhance the hole mobility for two-dimensional transport. In contrast, for in-plane tensile stress $\epsilon > 0$ (i.e., $a_s > a_0$) the top of the valence band is the in-plane heavy-hole state.[21,16]

(ii) Because the valence-band maximum changes its character as the strain changes sign, there is a change of slope of $E_g(\epsilon)$ about $\epsilon = 0$. Thus, the E_g vs ϵ curve has a "cusp" at $\epsilon = 0$ (Fig. 2). This is confirmed by experimental measurements.[20–25]

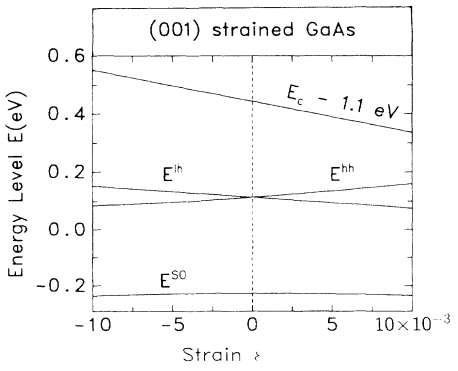

FIG. 1. Light-hole (lh), heavy-hole (hh), split-off (SO), and conduction-band (c) energy levels of (001) strained GaAs as function of strain $\epsilon = (a_s - a_0)/a_0$, where a_s and a_0 are the lattice constants of substrate and GaAs, respectively. Results are calculated from Eqs. (25) and (29) using the data of Table I. The energy zero is at the center of the valence band.

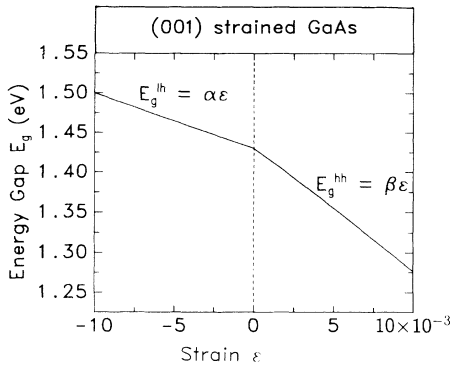

FIG. 2. Energy gap $E_c - E_{\rm VBM}$ of (001) strained GaAs as a function of strain ϵ. Note the change of slope at $\epsilon = 0$.

(iii) The lh slope α is much smaller than the hh slope β. Equation (28) shows that this is because the band-gap changes due to hydrostatic and shear strain add up for the $E_g^{\rm hh}$ gap (so β is large), while for the $E_g^{\rm lh}$ gap the two contributions tend to cancel each other (so α is small).

(iv) Our calculation shows that the slope (α or β) of the E_g vs ϵ curve is reduced significantly as the ratio $(C_{11}-C_{12})/C_{11}$ is reduced. The latter quantity is proportional to the ratio λ of bond-bending and bond-stretching force constants.[50,51] The reason is as follows. For fixed epitaxial strain ϵ, as λ is reduced the tetragonal distortion becomes larger [Eq. (20)], so the volume deformation $\frac{\Delta V}{V}$ becomes smaller. In addition, as λ decreases the deformation potential a is also reduced.[45,50] The reduction of $\frac{\Delta V}{V}$ and of a with decreasing λ leads to a reduction in the first term ("hydrostatic") of α and β [Eq. (28)]. This explains why the In-based III-V's ($\lambda \sim 0.15$)[50] have smaller α and β values than the Ga-based III-V's ($\lambda \sim 0.22$)[50] (Table I). We expect that α and β will be yet smaller for II-VI's where[50] $\lambda \sim 0.1$.

B. (001) strain with (111) CuPt ordering

We consider here an $A_xB_{1-x}C$ alloy with CuPt-type (111) order grown coherently on a (001) substrate. This is pertinent to most molecular-beam epitaxy and organometallic vapor-phase epitaxy experiments in which III-V alloys show CuPt ordering when grown on (001) substrates (see the review in Ref. 30). For this system the strain is measured by $\epsilon(x) = [a_s - a_f(x)]/a_f(x)$, where $a_f(x)$ and a_s are the lattice constants of the film and the substrate, respectively. The successive (111) ordering planes consist of an A-rich $A_{x+\frac{\eta}{2}}B_{1-x-\frac{\eta}{2}}$ and B-rich $A_{x-\frac{\eta}{2}}B_{1-x+\frac{\eta}{2}}$ layers, respectively, where η is the long range order parameter. All of our quantities are functions of ϵ and η. Our reference system is a strain-free, perfectly random alloy ($\eta = \epsilon = 0$) at the same composition. For example, the *band-gap reduction* is defined as $\Delta E_g(\eta, \epsilon) = E_g(\eta, \epsilon) - E_g(0, 0)$.

From the discussion of the previous section [Eqs. (17) and (29)], we see that for the conduction band

$$E_c(\eta,\epsilon) = E_g(\eta,0) + \tfrac{1}{3}[\Delta^{\rm SO} + \Delta^O_{111}(\eta)] - \tfrac{1}{2}(\alpha+\beta)\epsilon \ , \tag{30}$$

where $E_g(\eta,0)$ is the band gap of the strain-free alloy and $\Delta^O_{111}(\eta) > 0$ is the crystal field splitting due to (111) ordering. To a good approximation[34] both $E_g(\eta,0)$ and $\Delta^O_{111}(\eta)$ depend on η quadratically [Eq. (12)], so Eq. (30) can be expressed as

$$E_c(\eta,\epsilon) = E_g(0,0) + \eta^2\Delta E_g(1,0) + \tfrac{1}{3}[\Delta^{\rm SO} + \eta^2\Delta^O_{111}(1)] - \tfrac{1}{2}(\alpha+\beta)\epsilon \ . \tag{31}$$

The total Hamiltonian for the valence bands is constructed by combining Eqs. (7), (11), and (15). This gives

$$H_v = \frac{1}{3}\begin{pmatrix} \Delta^S_{001} & -\Delta^O_{111} - i\Delta^{\rm SO} & -\Delta^O_{111} & 0 & 0 & \Delta^{\rm SO} \\ -\Delta^O_{111} + i\Delta^{\rm SO} & \Delta^S_{001} & -\Delta^O_{111} & 0 & 0 & -i\Delta^{\rm SO} \\ -\Delta^O_{111} & -\Delta^O_{111} & -2\Delta^S_{001} & -\Delta^{\rm SO} & i\Delta^{\rm SO} & 0 \\ 0 & 0 & -\Delta^{\rm SO} & \Delta^S_{001} & -\Delta^O_{111} + i\Delta^{\rm SO} & -\Delta^O_{111} \\ 0 & 0 & -i\Delta^{\rm SO} & -\Delta^O_{111} - i\Delta^{\rm SO} & \Delta^S_{001} & -\Delta^O_{111} \\ \Delta^{\rm SO} & i\Delta^{\rm SO} & 0 & -\Delta^O_{111} & -\Delta^O_{111} & -2\Delta^S_{001} \end{pmatrix} . \tag{32}$$

where $\Delta^S_{001} = \frac{3}{2}(\alpha-\beta)\epsilon$ and $\Delta^O_{111} = \eta^2\Delta^O_{111}(1)$ are the crystal field splittings. The energy levels E_1, E_2, and E_3 (in decreasing order) can be obtained by diagonalizing Eq. (32).

For systems with no strain ($\epsilon = 0$), $\Delta^S_{001} = 0$, the three energy levels E_1 (with $\Gamma_{4,5}$ symmetry), E_2 (with Γ_6 symmetry), and E_3 (with Γ_6 symmetry) are given by an analytical form similar to that of Eq. (25). That is,

$$\begin{aligned} E_1(\eta,0) &= \frac{1}{3}[\Delta^{\rm SO} + \Delta^O_{111}(\eta)] \ , \\ E_2(\eta,0) &= -\frac{1}{6}[\Delta^{\rm SO} + \Delta^O_{111}(\eta)] \\ &\quad + \frac{1}{2}\sqrt{[\Delta^{\rm SO} + \Delta^O_{111}(\eta)]^2 - \frac{8}{3}\Delta^{\rm SO}\Delta^O_{111}(\eta)} \ , \\ E_3(\eta,0) &= -\frac{1}{6}[\Delta^{\rm SO} + \Delta^O_{111}(\eta)] \\ &\quad - \frac{1}{2}\sqrt{[\Delta^{\rm SO} + \Delta^O_{111}(\eta)]^2 - \frac{8}{3}\Delta^{\rm SO}\Delta^O_{111}(\eta)} \ . \end{aligned} \tag{33}$$

This corresponds to the case of *lattice matched* films. We have previously shown[34] that in this case one can measure $E_c(\eta,0) - E_1(\eta,0)$, $E_1(\eta,0) - E_2(\eta,0)$, and $E_1(\eta,0) - E_3(\eta,0)$ and fit to Eqs. (33) and (31), thus deducing the degree of order η. This procedure will be further illustrated in Figs. 7(b), 8(b), and 9(b) below.

In a more general case, there is a finite strain, so $\Delta^S_{001} \neq 0$ in Eq. (32). In the following we will use the $Ga_xIn_{1-x}P$ alloy as an example. The needed input data for evaluating Eqs. (31) and (32) are (i) the concentration-dependent properties $E_g(x)$, $a_f(x)$, $\Delta^{\rm SO}(x)$, $C_{ij}(x)$, $a(x)$, and $b(x)$ of the random alloy ($\eta = 0$) and (ii) the ordering-dependent properties $\Delta^O_{111}(1)$ and $\Delta E_g(1,0)$ of the fully ordered alloy. The first category of quantities are obtained for the random $Ga_xIn_{1-x}P$ alloy by assuming the usual quadratic bowing form

$$P(x) = xP({\rm GaP}) + (1-x)P({\rm InP}) - b_P x(1-x), \tag{34}$$

where b_P is the bowing parameter for property P. For the

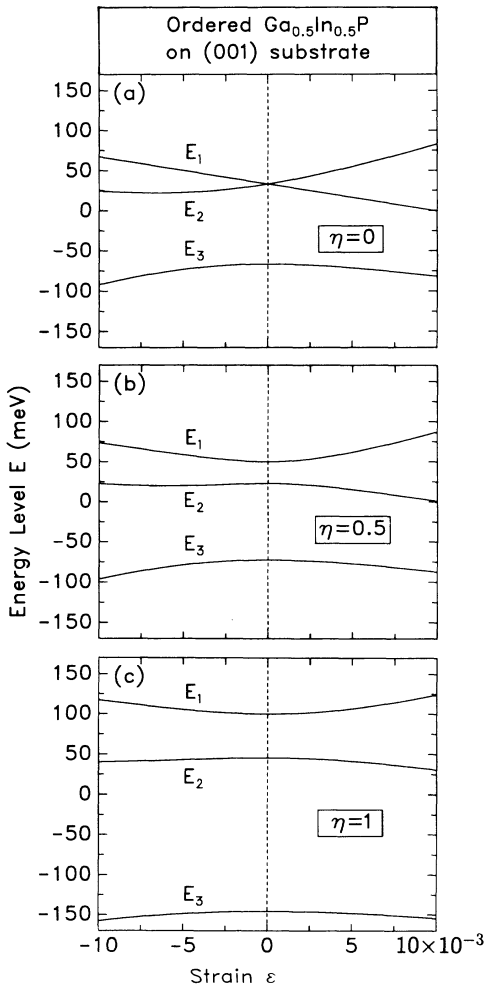

FIG. 3. The three valence-band energies E_1, E_2, and E_3 as functions of the strain ϵ and ordering parameters η for (001) strained $Ga_{0.5}In_{0.5}P$ with (111) ordering at (a) $\eta = 0$; (b) $\eta = 0.5$; and (c) $\eta = 1$. Results are calculated from Eq. (32) using the data from Table I and Ref. 34.

spin-orbit splitting we use the bowing[34] $b_{\Delta so} = -0.02$ eV, while for the direct band gap the bowing is[45] $b_{E_g} = 0.76$ eV. We assume zero bowing for lattice constant, elastic constants, and deformation potentials. These input values for $Ga_xIn_{1-x}P$ are given in Table I. For the second category of quantities, we use our previously calculated band structure values[34] $\Delta^O_{111}(1) = 0.20$ eV and $\Delta E_g(1,0) = -0.32$ eV.

In what follows we will explore two ways of exerting strain. First (Sec. III B 1) we will assume a $Ga_{0.5}In_{0.5}P$ film of fixed composition $x = 0.5$ being grown on (001) alloy substrates with varying lattice constants a_s. The biaxial strain is $\epsilon(a_s) = [a_s - a_f(0.5)]/a_f(0.5)$, where $a_f(0.5)$ is the lattice constant of the the equimolar film. Second (Sec. III B 2), we will consider the more common situation[20–25] of a variable composition $Ga_xIn_{1-x}P$ film with lattice constant $a_f(x)$, being grown coherently on a fixed GaAs (001) substrate with $a_s = 5.6533$ Å. In this case, the biaxial strain is $\epsilon(x) = [a_s(\text{GaAs}) - a_f(x)]/a_f(x)$. Note that in the second case the properties of the film vary because of changes in strain *and* composition, while in the first case there are only strain-induced changes.

1. *Equimolar $Ga_{0.5}In_{0.5}P$ on a (001) substrate*

Using the data of Table I we have diagonalized Eq. (32) and plotted in Fig. 3 the three valence-band energies E_1, E_2, and E_3 as functions of the strain ϵ at three different (111) ordering parameters η. Note that Fig. 3(a) (no ordering) is analogous to Fig. 1. We have also plotted the band gap E_g (Fig. 4) and the valence-band splitting $\Delta E_{12} = |E_1 - E_2|$ (Fig. 5), respectively as functions of ϵ and η for $Ga_{0.5}In_{0.5}P$. From these plots we find the following.

(i) When $\eta = 0$ (no ordering), both E_g (Fig. 4) and the valence-band splitting ΔE_{12} (Fig. 5) have a cusp at $\epsilon = 0$. This cusp results from E^{lh} and E^{hh} switching order at $\epsilon = 0$. Figures 4 and 5 show that this cusp is removed if $\eta \neq 0$. This is so since any amount of atomic order will mix equal amounts of lh and hh states at $\epsilon = 0$, so $\frac{\partial E_{12}}{\partial \epsilon}|_{(\epsilon=0;\eta\neq 0)} = 0$. This should be observed experimentally. The rounding of the cusp of ΔE_{12} vs ϵ could be used as an indirect measure of atomic ordering.

(ii) (001) strain always increases the valence-band splitting ΔE_{12} relative to the pure (111) ordering, and vice versa (Fig. 5). This is because the (001) and the (111) deformation potentials can be considered as complementary [Eq. (32)], so the combined effect is always larger than the individual ones.

(iii) (111) atomic ordering not only reduces the band gaps[32,33] (Fig. 4), but it also reduces the slope $\frac{\partial E_{12}}{\partial \epsilon}$ (Fig. 5). This reflects an increases in the mixing of the E^{lh} and E^{hh} strain components. This too can be used as an indirect measure of atomic ordering.

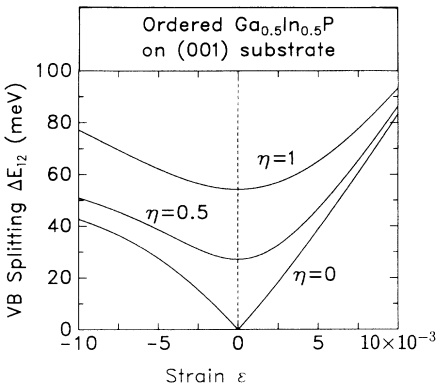

FIG. 5. Valence-band splitting $\Delta E_{12} = |E_1 - E_2|$ as a function of strain ϵ and ordering parameter η for (001) strained $Ga_{0.5}In_{0.5}P$ with (111) ordering at $\eta = 0$, 0.5, and 1.

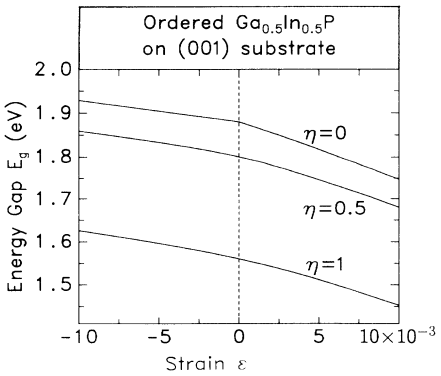

FIG. 4. Band gap E_g as a function of strain ϵ and ordering parameter η for (001) strained $Ga_{0.5}In_{0.5}P$ with (111) ordering at $\eta = 0$, 0.5, and 1. Results are calculated from Eqs. (31) and (32) using the data from Table I and Ref. 34.

2. *$Ga_xIn_{1-x}P$ on GaAs (001) substrate*

In this case the strain is caused by lattice mismatch between the $Ga_xIn_{1-x}P$ film and the GaAs substrate.

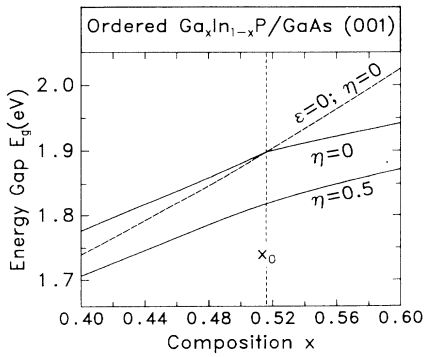

FIG. 6. Band-gap energy of the strained $Ga_xIn_{1-x}P$ as a function of composition x at $\eta = 0$ and $\eta = 0.5$. The band-gap energy of the strain-free random alloy is also plotted (dashed line) using the relation $E_g(x) = 2.78x + 1.35(1-x) - 0.76x(1-x)$ (Ref. 45).

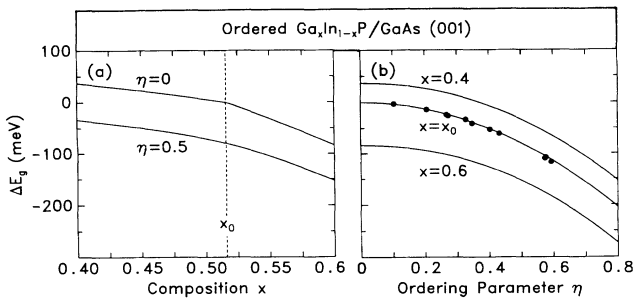

FIG. 7. Band-gap reduction $\Delta E_g[\eta, \epsilon(x)] = E_g[\eta, \epsilon(x)] - E_g[0,0]$ of the strained $Ga_xIn_{1-x}P$ alloy as a function of (a) composition x and (b) long range order parameter η. The experimental data of Ref. 35 are plotted as solid dots in (b).

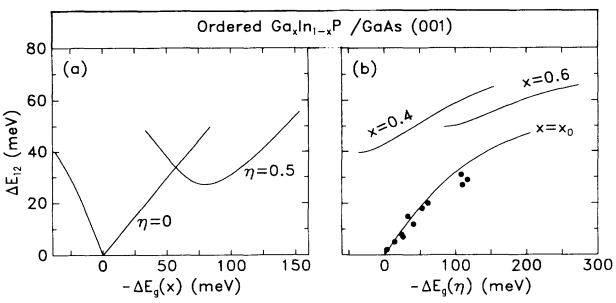

FIG. 9. Correlation between ΔE_{12} and ΔE_g. (a) Varying composition x at fixed long range order parameter η. (b) Varying long range order parameter η at fixed composition. The experimental data of Ref. 35 are plotted as solid dots in (b).

This strain $\epsilon(x)$ is a function of the film composition x, and so are the other composition-dependent properties $P(x)$ for the strain-free random alloy. We use Vegard's rule[52] to determine the equilibrium lattice constant $a_f(x)$ and assume that at fixed composition x ordering does not change the lattice constant. Using the lattice parameters from Table I, the strain-free composition is calculated to be at $x_0 = 0.516$. Using the data of Table I, the composition dependence of the input parameters given by Eq. (34), and the Hamiltonians [Eqs. (31) and (32)], we have plotted in Fig. 6 the band-gap energy of the $Ga_xIn_{1-x}P$ film as a function of the composition x at $\eta = 0$ and $\eta = 0.5$. This figure also shows the band gap of the strain-free random alloy (dashed line). Figure 7 shows the band-gap reduction $\Delta E_g(\eta, \epsilon)$. Part (a) of this figure shows dependence on composition, while part (b) shows the dependence on the degree of ordering. Figure 8 shows the valence-band splitting $\Delta E_{12}(\eta, \epsilon)$ as a function of composition [Fig. 8(a)] and ordering [Fig. 8(b)]. We see that

(i) In the absence of ordering strain can either increase (for $x < x_0$) or decrease (for $x > x_0$) the band gap [Figs. 6 and 7(a)]. On the other hand, ordering ($\eta > 0$) always reduces the band gap [Fig. 7(b)]. The change is parabolic, i.e., $\Delta E_g \propto \eta^2$.

(ii) Ordering ($\eta > 0$) and strain ($x \neq x_0$) both increase the valence-band splitting ΔE_{12} (Fig. 8). For fixed η, the valence-band splitting ΔE_{12} has a minimum at x_0 [Fig. 8(a)]. For small η the valence-band splitting is dominated by strain [Fig. 8(b)]. When the degree of ordering increases, the splitting increases and the effect of strain is reduced.

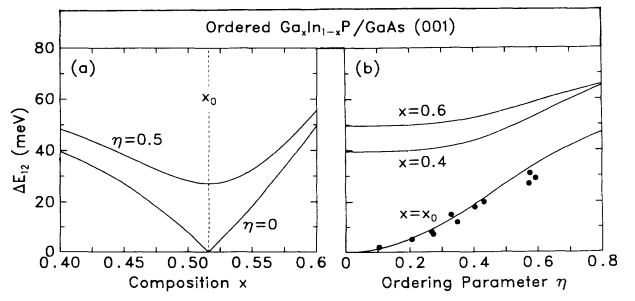

FIG. 8. Valence-band splitting ΔE_{12} of the strained $Ga_xIn_{1-x}P$ alloy as a function of (a) composition x and (b) the long range order parameter η. The experimental data of Ref. 35 are plotted as solid dots in (b).

The predictions of Fig. 7(b) (ΔE_g vs η) and Fig. 8(b) (ΔE_{12} vs η) have been used in the past[34] to extract from reflectivity experiments the value of the long range order (LRO) parameter. This was done by fitting ΔE_g and ΔE_{12} of a given sample to Eqs. (31) and (33) and extracting η. The solid dots in Fig. 7(b) and 8(b) (data taken from Ref. 35) represent such a fit. In this case the data apply to $x = x_0$. We now extend such ideas to strained samples. Figure 9 shows the correlation between ΔE_{12} and ΔE_g for varying compositions at some fixed degree of LRO (a) and for varying degree of LRO at some fixed composition (b). Figure 9(a) demonstrates that one can have a valence-band splitting *and* a valence gap reduction even without ordering ($\eta = 0$), but that ordering modifies the ΔE_{12} vs ΔE_g dependence considerably. Figure 9(b) shows that *without* strain ($x = x_0$) we expect a simple nearly parabolic increase of $|\Delta E_g|$ with increasing ΔE_{12}. The experimental data points of Alonso *et al.*[35] are depicted in this figure on the $x = x_0$ curve. We see a good agreement for low $|\Delta E_g|$ values, but the measured high $|\Delta E_g|$ values are slightly *below* the calculated line. Figure 9(b) indicate that strain *cannot* be the reason for this discrepancy since any value of $x \neq x_0$ will further displace ΔE_{12} to *higher* values. A possible explanation is clustering-type short range order (SRO): such clustering was recently predicted[53] to reduce the band gap (larger $|\Delta E_g|$) without introducing a crystal field splitting. Indeed, cluster-type SRO was detected in many alloys.[54–57] It hence appears that simultaneous measurements of ΔE_{12} and ΔE_g could be used along with our theory to discern the effects of LRO, SRO, and strain.

IV. OPTICAL TRANSITION PROBABILITIES AND POLARIZATION

We have seen that both strain and ordering reduce the symmetry of the crystal, splitting the Γ_{8v} state of the

strain-free random alloy into two states, labeled $|1\rangle$ and $|2\rangle$. We use the convention that the energy of $|1\rangle$ is higher than energy of $|2\rangle$. In this section we discuss the way that strain and ordering affect the intensities of the transition between $|1\rangle$, $|2\rangle$, and the conduction-band minimum.

The transition probability between conduction state Ψ_c and valence state Ψ_v is determined by the the matrix element of the transition $\langle\Psi_c|H_{\rm int}|\Psi_v\rangle$, where $H_{\rm int}$ is the interacting Hamiltonian. For *linearly* polarized light along the $[l,m,n]$ direction we have $H_{\rm int} \propto lx+my+nz$, while for *circularly* polarized light $\sigma^{\pm}$ with angular momentum parallel and antiparallel to z' we have[58] $H_{\rm int} \propto x' \pm iy'$. In general, for polarized light $H_{\rm int}$ can be expressed as a linear combination of $x_\mu = x$, y, or z. The transition intensity is proportional to $I_{v,c} = |\langle\Psi_c|H_{\rm int}|\Psi_v\rangle|^2$. Note that, due to phase correlation, the transition intensity for coherent, linearly polarized light, e.g., $H_{\rm int} = c(x+y)$, is different from the sum of the intensities for the two incoherent polarized light $H_{\rm int} = cx$ and $H_{\rm int} = cy$. (In Ref. 59 and Ref. 60 errors were made in the intensity analysis by making the erroneous assumption that $|\langle\Psi_c|x+y|\Psi_v\rangle|^2 = |\langle\Psi_c|x|\Psi_v\rangle|^2 + |\langle\Psi_c|y|\Psi_v\rangle|^2$).

We calculate the valence eigenstates Ψ_v by diagonalizing the Hamiltonian in the form of Eq. (32). This produces a linear combination of the basis function $\{p_\nu\hat{\sigma}\}$, where $p_\nu = x$, y, or z are the $L=1$ orbital components and $\hat{\sigma}$ are the spinors parallel or antiparallel to the z direction. The conduction states are taken here as $\Psi_c = s\hat{\sigma}$, where s is the $L=0$ orbital component. In doing this we have neglected the mixing between the conduction s state and the valence p state. The transition matrix elements can be obtained by writing the orbital wave functions and $H_{\rm int}$ in terms of the spherical harmonics Y_{lm} and by noticing that the allowed dipole transitions are for $\Delta m = \pm 1$. This gives the simple selection rule[58,61]

$$\langle s\hat{\sigma} \mid x_\mu \mid p_\nu\hat{\sigma}'\rangle = c\,\delta_{\mu,\nu}\delta_{\hat{\sigma},\hat{\sigma}'}\,, \tag{35}$$

where c is a normalization parameter.

Using Eq. (35) we have calculated the transition intensity $I_{v,c}$ between the $|1\rangle$ and $|2\rangle$ valence states and the conduction state in $Ga_{0.5}In_{0.5}P$ as a function of (001) strain ϵ and $(\bar{1}11)$ ordering parameter η. [The $(\bar{1}11)$ and $(1\bar{1}1)$ ordering are the two subvariants of "$CuPt_B$" observed for this system. The other two subvariants (111) and $(11\bar{1})$ of "$CuPt_A$" are not seen experimentally.[30]] Note that to compare $I_{v,c}$ with experimentally measured intensities we should also include line broadening, joint density of states, and temperature factors.

We apply linearly polarized light with polarization $\hat{e} \parallel [1\bar{1}0]$ (defined as $\Theta = 0$); $\hat{e} \parallel [110]$ (defined as $\Theta = 90°$); and in between. The calculated intensities for these linearly polarized light are the same for the two $CuPt_B$ subvariants. For the two $CuPt_A$ subvariants the role of [110] and $[1\bar{1}0]$ polarization is switched. We find the following results.

A. Pure (001) strain ($\eta = 0$)

(001) strain splits the Γ_{8v} VBM into Γ_{6v} and Γ_{7v}. The energy of Γ_{6v} is above Γ_{7v} for $\epsilon < 0$ and below it for

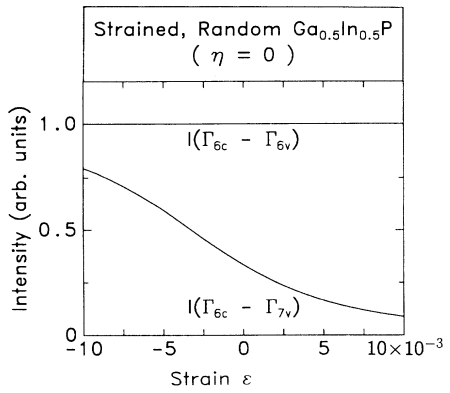

FIG. 10. Calculated transition intensities (in arbitrary units) of the random ($\eta = 0$) $Ga_{0.5}In_{0.5}P$ alloy as a function of (001) strain ϵ. The intensity is independent of the polarization angle Θ.

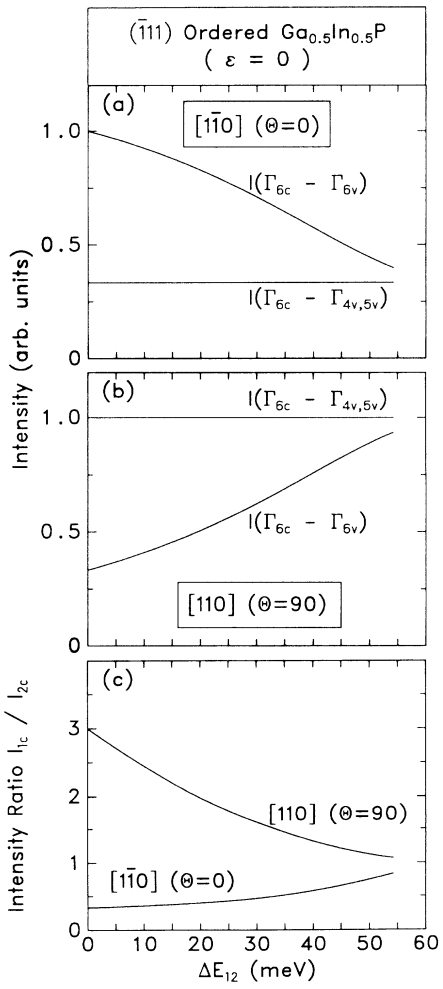

FIG. 11. Calculated transition intensities for $(\bar{1}11)$ ordered, strain-free ($\epsilon = 0$) $Ga_{0.5}In_{0.5}P$ as a function of the valence-band splitting ΔE_{12} for (a) light polarized along $[1\bar{1}0]$ and (b) light polarized along [110]. (c) gives the intensity ratio $I(\Gamma_{6c}\text{-}\Gamma_{4v,5v})/I(\Gamma_{6c}\text{-}\Gamma_{6v})$.

$\epsilon > 0$. We thus have the $\Gamma_{6c} - \Gamma_{6v}$ and the $\Gamma_{6c} - \Gamma_{7v}$ transitions. For pure (001) strain both transition intensities are independent of the polarization angle Θ. If one further assumes zero s-p wave-function mixing, the intensity $I(\Gamma_{6c}\text{-}\Gamma_{6v})$ is also strain-independent (Fig. 10). The intensity $I(\Gamma_{6c}\text{-}\Gamma_{7v})$, however, does depend on strain due to the coupling between the Γ_{7v} state and the split-off state, which also has Γ_{7v} symmetry. Figure 10 shows that the intensity $I(\Gamma_{6c}\text{-}\Gamma_{7v})$ decreases when strain changes from negative to positive. We are unaware of experimental observations of such strain-dependent optical transition intensity in cubic materials.

B. Pure ($\bar{1}11$) CuPt ordering ($\epsilon = 0$)

Pure ($\bar{1}11$) ordering (i.e., no strain) splits the Γ_{8v} VBM into $|1\rangle = \Gamma_{4v,5v}$ and $|2\rangle = \Gamma_{6v}$ states. In this case the transition probability depends on the polarization angle, since relative to the [$\bar{1}11$] ordering axis the two polarization directions [$1\bar{1}0$] and [110] are inequivalent. Figure 11 shows the calculated intensity for the transitions $\Gamma_{4v,5v}$-Γ_{6c} and Γ_{6v}-Γ_{6c} as functions of ΔE_{12} for polarization $\hat{e} \parallel [1\bar{1}0]$ (a) and $\hat{e} \parallel [110]$ (b). [The valence-band splitting ΔE_{12} can be obtained from Eq. (33) as a function of the ordering parameter η.] As we see from Figs. 11(a) and 11(b) the intensity $I(\Gamma_{6c}\text{-}\Gamma_{4v,5v})$ does not depend on ΔE_{12} since there is no coupling between this state and the other two valence states (both have the Γ_{6v} symmetry). In contrast, the intensity $I(\Gamma_{6c}\text{-}\Gamma_{6v})$ depends strongly on ΔE_{12}, because the coupling of the two Γ_{6v} states depends on the degree of ordering, and thus on ΔE_{12}.

We will distinguish in what follows two coupling limits, the quasicubic limit when $\Delta^{O}_{\bar{1}11} << \Delta^{\mathrm{SO}}$ and the trigonal limit when $\Delta^{O}_{\bar{1}11} >> \Delta^{\mathrm{SO}}$. In the quasicubic regime we have $\Delta E_{12} \approx 0$. In this limit the polarization ratio is [Fig. 11(c)]

$$\frac{I(\Gamma_{6c}\text{-}\Gamma_{4v,5v})}{I(\Gamma_{6c}\text{-}\Gamma_{6v})} = \begin{cases} \frac{1}{3}, & \hat{e}\|[1\bar{1}0]\ , \\ 3, & \hat{e}\|[110]\ . \end{cases} \tag{36}$$

In this "weak ordering" regime, $|1\rangle$ and $|2\rangle$ are nearly degenerate, so only the combined intensity $I(\Gamma_{6c}\text{-}\Gamma_{4v,5v}) + I(\Gamma_{6c}\text{-}\Gamma_{6v})$ can be measured. For $\Delta E_{12} = 0$ this total intensity is the same for the [110] or the [$1\bar{1}0$] polarization [Figs. 11(a) and 11(b)], as appropriate for a cubic system. Thus, no polarization dependence can be detected if the two transitions are not resolved. As the degree of order (thus, ΔE_{12}) increases the intensity ratio $I(\Gamma_{6c}\text{-}\Gamma_{4v,5v})/I(\Gamma_{6c}\text{-}\Gamma_{6v})$ approaches unity for both polarization directions. In the extreme trigonal limit [Fig. 11(c)]

$$\frac{I(\Gamma_{6c}\text{-}\Gamma_{4v,5v})}{I(\Gamma_{6c}\text{-}\Gamma_{6v})} = \begin{cases} 1, & \hat{e}\|[1\bar{1}0]\ , \\ 1, & \hat{e}\|[110]\ , \end{cases} \tag{37}$$

and the polarization dependence is given by [Figs. 11(a) and 11(b)]

$$\frac{I[110]}{I[1\bar{1}0]} = 3\ . \tag{38}$$

Note that Alsina *et al.*[60] neglected the coupling between the two Γ_{6v} states in the trigonal regime and replaced coherent polarized light with incoherent polarized light. Instead of obtaining the ratio of Eq. (37), they incorrectly found the ratio $I(\Gamma_{6c}\text{-}\Gamma_{4v,5v})/I(\Gamma_{6c} - \Gamma_{6v}) = 1/5$ for the [$1\bar{1}0$] polarization.

Figure 12 depicts the calculated normalized intensities as functions of the polarization angle Θ. We find that the intensity can be described by

$$I(\Theta) = I_{110}\sin^2\Theta + I_{1\bar{1}0}\cos^2\Theta. \tag{39}$$

For the Γ_{6c}-$\Gamma_{4v,5v}$ transition [Fig. 12(a)] the intensity is independent of η. For the Γ_{6c}-Γ_{6v} transition, however, we see a strong dependence on the ordering parameter η. $I(\Theta)$ can either be an increasing function (at large η) or a decreasing function (at small η) of the polarization angle Θ. Figure 12 compares our calculated results (lines) with the recent polarized electroreflectance data of Kanata *et al.*[59] (solid dots). We find that the best fit to the data can be obtained using $\eta = 0.58$, which corresponds (see Fig. 8) to a valence-band splitting of $\Delta E_{12} = 34$ meV. The measured[59] valence-band splitting is $\Delta E_{12} = 34 \pm 4$

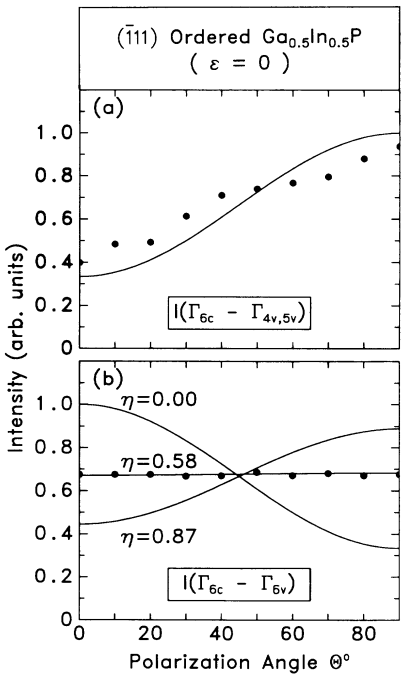

FIG. 12. Calculated normalized transition intensity of ($\bar{1}11$) ordered $Ga_{0.5}In_{0.5}P$ as a function of polarization angle Θ. Here, $\Theta = 0$ denotes light polarized along [$1\bar{1}0$], while $\Theta = 90°$ denotes light polarized along [110]. (a) The Γ_{6c}-$\Gamma_{4v,5v}$ transition. The intensity is independent of η. (b) The Γ_{6c}-Γ_{6v} transition at $\eta = 0.00$, 0.58, and 0.87. The corresponding ΔE_{12} are 0, 34, and 50 meV, respectively. The solid dots in (a) and (b) are the experimental data of Kanata *et al.* (Ref. 59).

meV, in excellent agreement with the above value. The small discrepancy between the data and the theoretical line of Fig. 12(a) is possibly because the incident angle of the light in the experiment[59] is not exactly perpendicular to the (001) surface. It may also be due to a small strain in the sample (see below).

In most previous analyses of experimental data[35,36,59,62], the intensity ratio of the quasicubic limit [Eq. (36)] was applied to *all* degrees of ordering. The ordering dependence of the intensity ratio was thus missed. As we seen in Figs. 11(c) and 12(b) this assumption could introduce large errors.

C. Coexistence of ordering ($\eta \neq 0$) and strain ($\epsilon \neq 0$)

In the presence of both ordering and strain, the wave functions at the top of the valence bands have mixed (001) and ($\bar{1}11$) character. The symmetry of the crystal is reduced to monoclinic. We will simply denote the states as $|1\rangle$ and $|2\rangle$. The transition intensities are determined by the relative strengths of the ordering and strain. Figure 13 shows the calculated transition intensities of strained $Ga_{0.5}In_{0.5}P$ as functions of ΔE_{12} for [1$\bar{1}$0] polarized light (solid lines). For comparison, we show as dashed lines the transition intensities for pure ordering without strain. We use the strain-induced crystal field splitting $\Delta_{001}^{S} = +10$ meV [Fig. 13(a)] and -10 meV [Fig. 13(b)], which correspond to $\epsilon = -0.1\%$ and $\epsilon = +0.1\%$, respectively.

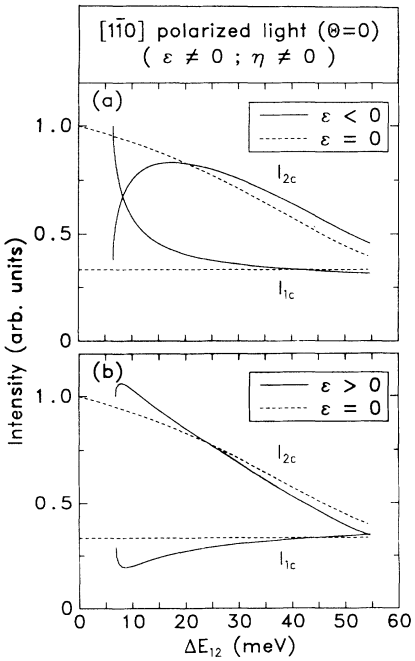

FIG. 13. Strain effects on the transition intensities for ($\bar{1}11$) ordered $Ga_{0.5}In_{0.5}P$ as a function of ΔE_{12} for [1$\bar{1}$0] polarized light. Solid lines are for (001) strain (a) $\epsilon = -0.1\%$, (b) $\epsilon = +0.1\%$. The dashed lines are the results for strain-free ($\epsilon = 0$) ordered samples [see Fig. 11(a)].

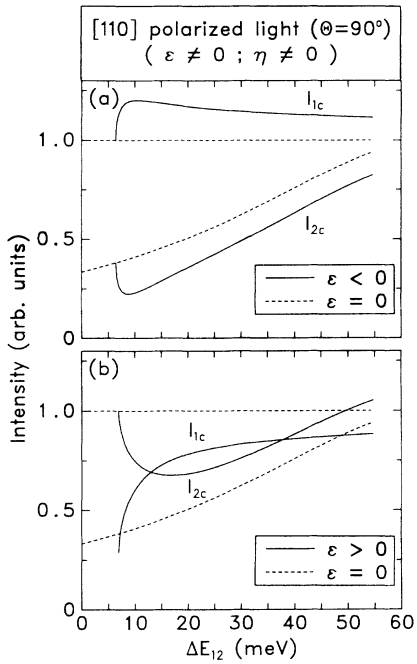

FIG. 14. Strain effects on the transition intensities for ($\bar{1}11$) ordered $Ga_{0.5}In_{0.5}P$ as a function of ΔE_{12} for [110] polarized light. Solid lines are for (001) strain (a) $\epsilon = -0.1\%$, (b) $\epsilon = +0.1\%$. The dashed lines are the results for strain-free ($\epsilon = 0$) ordered samples [see Fig. 11(b)].

For weak ordering and *zero* strain Fig. 13(a) shows that $I_{1,c}/I_{2,c} \sim 1/3$. But with a small strain $\epsilon < 0$, the ratio changes to ~ 3. This result indicates that, when strain-induced crystal field splitting is comparable to the ordering-induced crystal field splitting, an accurate analysis of the observed transition intensity could be difficult. When the degree of ordering (thus, ΔE_{12}) increases, the transition intensities approach the $\epsilon = 0$ values for "pure ordering" (Fig. 13).

Similar results are plotted in Fig. 14 for [110] polarization. Comparing to the results for [1$\bar{1}$0] polarized light (Fig. 13), we see that the effects of positive and negative strain are reversed and that the change of intensity due to strain is larger in the case of $\hat{e} \parallel [110]$. Figures 13 and 14 also suggest that for $\epsilon > 0$ it is better to use [1$\bar{1}$0] polarized light to study ordering-induced effects, while for $\epsilon < 0$ it is better to use [110] polarized light.

D. Spin polarization

It is interesting to study the ordering-induced changes in spin polarization of emitted photoelectrons. We use for this purpose circularly polarized light.[58,63,64] For circularly polarized light $\sigma^{\pm}$ with its angular momentum along the ordering direction [$\bar{1}$11] we have $H_{\rm int} \propto x' \pm iy'$, where $x' = \frac{1}{\sqrt{2}}(x+y)$ and $y' = \frac{1}{\sqrt{6}}(-x+y-2z)$. The spinors parallel and antiparallel to the [$\bar{1}$11] ordering direction are given by

$$\uparrow' = \cos\frac{\theta}{2}e^{-i\frac{\varphi}{2}}\uparrow + \sin\frac{\theta}{2}e^{i\frac{\varphi}{2}}\downarrow ,$$

$$\downarrow' = -\sin\frac{\theta}{2}e^{-i\frac{\varphi}{2}}\uparrow + \cos\frac{\theta}{2}e^{i\frac{\varphi}{2}}\downarrow , \tag{40}$$

where the angles θ and φ are determined by the equation $(\sin\theta\cos\varphi, \sin\theta\sin\varphi, \cos\theta) = \frac{1}{\sqrt{3}}(\bar{1}, 1, 1)$. The $\uparrow$ and $\downarrow$ are the spinors parallel and antiparallel to the [001] direction, respectively. The electron spin polarization P is defined as[58,63,64]

$$P = \frac{I_- - I_+}{I_- + I_+} , \tag{41}$$

where I_- and I_+ are the transition intensities for $\downarrow'$ spin and $\uparrow'$ spin, respectively. In Fig. 15 we show the calculated spin intensities $(I_- - I_+)_{1c}$ and $(I_- - I_+)_{2c}$ for strain-free ordered $Ga_{0.5}In_{0.5}P$ alloys (dashed lines). For the random alloy ($\eta = \Delta E_{12} = 0$) the states $|\,1\rangle$ and $|\,2\rangle$ are degenerate. In this case, we find that optical pumping from both states leads to a $P = 50\%$ electron spin polarization.[58] For the ordered alloy ($\eta \neq 0$), the $|\,1\rangle = \Gamma_{4v,5v}$ and $|\,2\rangle = \Gamma_{6v}$ states split. We find that photoelectrons generated from the $\Gamma_{4v,5v}$ and the Γ_{6v} states are both fully polarized. Hence, if the splitting ΔE_{12} is large enough to allow optical pumping only from the highest $\Gamma_{4v,5v}$ state, the generated photoelectrons can be 100% spin polarized. A theoretical 100% spin polarization of electrons can also be achieved by using (001) ordered material [with spin parallel to the (001) direction], as proposed in Ref. 63 and tested in Ref. 65. However, since the (111) ordered material has much larger valence-band splitting than (001) ordered samples,[33] we suggest that (111) ordered III-V alloys (e.g., $Ga_{0.5}In_{0.5}P$) could be better candidates for a spin-polarized photoelectron source.

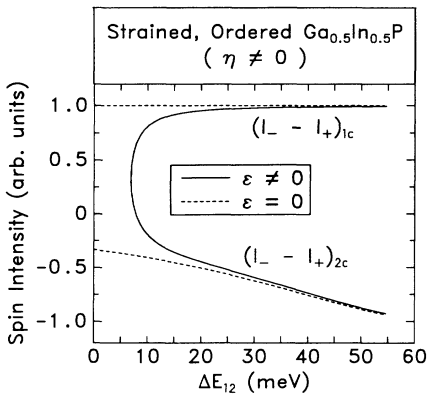

FIG. 15. Calculated spin intensity $(I_- - I_+)_{1c}$ and $(I_- - I_+)_{2c}$ (in arbitrary units) of ordered $Ga_{0.5}In_{0.5}P$ as a function of ΔE_{12}. The angular momentum of the circularly polarized light is in the same direction as the ordering vector. The dashed lines are the results for a strain-free ($\epsilon = 0$) ($\bar{1}11$) ordered alloy. In this case, the generated photoelectron from each band is fully polarized. The solid lines are the results for ($\bar{1}11$) ordered samples with (001) strain $\epsilon = \pm 0.1\%$. The results are not sensitive to the sign of the strain.

Note that, despite the identical optical response with respect to the linearly polarized light along [110] and [$1\bar{1}0$] of the two $CuPt_B$ [($1\bar{1}1$) and ($\bar{1}11$)] subvariants, their responses to the circularly polarized light are different. Using the same σ^+ light noted above but for ($1\bar{1}1$) ordering, we find that the spin polarization P for the transition from the top $\Gamma_{4v,5v}$ state is only 20% and the total intensity $I_- + I_+$ is reduced to 55.56% of the intensity for ($\bar{1}11$) ordering. This difference can be used to distinguish ($1\bar{1}1$) ordering from ($\bar{1}11$) ordering, which is not possible using linearly polarized light. This also indicates that, in order to obtain the highest efficiency in generating spin polarized electrons, single-variant crystals are required.

To see the effects of strain on the spin polarization, we show in Fig. 15 the spin intensity of ordered $Ga_{0.5}In_{0.5}P$ alloys with strain (solid lines). The applied (001) strains are $\epsilon = \pm 0.1\%$. For pure (001) strain ($\eta = 0$) the spin of the photoelectron generated from the VBM is fully polarized along the [001] direction. Its projection on the [$\bar{1}11$] axis reduces the polarization to only 50%. As the degree of ordering increases, the spin polarization along the [$\bar{1}11$] axis increases rapidly and become similar to the one for the purely ordered sample. The results, unlike the ones for linearly polarized light, are essentially independent of the *sign* of the strain.

V. SUMMARY OF EXPERIMENTALLY TESTABLE PREDICTIONS

The theory outlined in this paper makes a number of testable predictions:

(i) The degree η of LRO can be obtained by measuring ΔE_{12} and ΔE_g and fitting the results to Figs. 7 and 8. This was previously done[34] for the lattice matched composition x_0.

(ii) Ordering can be detected by measuring the band gap vs x: as Fig. 6 shows, the cusp disappears with ordering. The same is true for ΔE_{12} measurements (Fig. 8). The slopes (α and β) of E_g vs ϵ are expected to be smaller for more ionic II-VI's.

(iii) It is useful to plot measured ΔE_g vs ΔE_{12} [Fig. 9(b)] for a *range* of compositions near $x = x_0$. There are three domains in this plane. If the measured data fall *on* the $x = x_0$ line one can conclude that *atomic ordering* is the cause of both ΔE_g and ΔE_{12}. If the data fall *above* the calculated $x = x_0$ line, *epitaxial strain* should be considered. If the data fall *below* the $x = x_0$ line, one should suspect clustering and attempt to measure it directly.[54–57]

(iv) Ordering induces anisotropy in the optical transition intensities. By measuring the relative transition intensity of the sample, one can determine the ordering vectors using linearly polarized light (separating $CuPt_A$ from $CuPt_B$) and circularly polarized light [separating the subvariant ($\bar{1}11$) from ($1\bar{1}1$) ordering].

(v) Optical transition intensity analysis can be used to determine the size of the strain (Fig. 10), the degree of ordering (Figs. 11 and 12), or both (Figs. 13 and 14).

(vi) A single-variant CuPt-like ordered material can be used as a good spin-polarized photoelectron source.

ACKNOWLEDGMENTS

We thank Kurt Mader for helpful discussions. This work was supported in part by the U.S. Department of Energy, OER-BES, Grant DE-AC02-83-CH10093.

[1] G. E. Pikus and G. L. Bir, Fiz. Tverd. Tela (Leningrad) **1**, 154, (1959); **1**, 1642 (1959); **3**, 1001 (1961) [Sov. Phys. Solid State **1**, 136 (1959); **1**, 1502 (1959); **3**, 730 (1961)]; Phys. Rev. Lett. **6**, 103 (1961).
[2] W. H. Kleiner and L. M. Roth, Phys. Rev. Lett. **2**, 334 (1959).
[3] J. C. Hensel and G. Feher, Phys. Rev. **129**, 1041 (1963).
[4] F. H. Pollak and M. Cardona, Phys. Rev. **172**, 816 (1968).
[5] E. O. Kane, Phys. Rev. **178**, 1368 (1969).
[6] F. Cerdeira, C. J. Buchenauer, F. H. Pollak, and M. Cardona, Phys. Rev. B **5**, 580 (1972).
[7] M. Chandrasekhar and F. H. Pollak, Phys. Rev. B **15**, 2127 (1977).
[8] A. Blacha, H. Presting, and M. Cardona, Phys. Status Solidi B **126**, 11 (1984), and references therein.
[9] W. Pötz and P. Vogl, Phys. Rev. B **24**, 2025 (1981).
[10] O. H. Nielsen and R. M. Martin, Phys. Rev. B **32**, 3792 (1985).
[11] R. G. Dandrea and A. Zunger, Phys. Rev. B **43**, 8962 (1991).
[12] D. Bertho, D. Boiron, A. Simon, C. Jouanin, and C. Priester, Phys. Rev. B **44**, 6118 (1991).
[13] T. Nakayama, in *Proceedings of the 9th International Conference on Physics of Ternary and Multinary Compounds, Yokohama, Japan, 1993* [Jpn. J. Appl. Phys. (to be published)].
[14] G. A. Baraff and D. Gershoni, Phys. Rev. B **43**, 4011 (1991).
[15] R. People, Phys. Rev. B **32**, 1405 (1985).
[16] R. People, Appl. Phys. Lett. **50**, 1604 (1987).
[17] C. G. Van de Walle, Phys. Rev. B **39**, 1871 (1989).
[18] M. Silver, W. Batty, A. Ghiti, and E. P. O'Reilly, Phys. Rev. B **46**, 6781 (1992).
[19] T. Saka, T. Kato, T. Nakanishi, H. Aoyagi, T. Kosugoh, S. Nakamura, M. Tawada, M. Tsubata, H. Horinaka, and Y. Kamiya, J. Cryst. Growth **124**, 346 (1992).
[20] H. Asai and K. Oe, J. Appl. Phys. **54**, 2052 (1983).
[21] C. P. Kuo, S. K. Vong, R. M. Cohen, and G. B. Stringfellow, J. Appl. Phys. **57**, 5428 (1985).
[22] T. Kato, T. Matsumoto, M. Hosoki, and T. Ishida, Jpn. J. Appl. Phys. **26**, L1597 (1987).
[23] D. Moroni, E. Dupont-Nivet, J. P. Andre, J. N. Patillou, and C. Delalarde, J. Appl. Phys. **63**, 5188 (1988).
[24] J. P. Ardre, E. Augarde, E. Dupont-Nivet, J. N. Patillou, P. Riglet, N. Mariel, D. Moroni, and A. Valster, Prog. Cryst. Growth Charact. **19**, 97 (1989).
[25] K. Ozasa, M. Yuri, S. Tanaka, and H. Matsunami, J. Appl. Phys. **68**, 107 (1990).
[26] D. Gershoni and H. Temkin, J. Lumin. **44**, 381 (1989).
[27] V. Lemos, C. Vazquez-Lopez, and F. Cardeira, Superlatt. Microstruct. **13**, 189 (1993).
[28] T. P. Pearsall, J. Lumin. **44**, 367 (1989).
[29] T. P. Pearsall, F. H. Pollak, J. C. Bean, and R. Hull, Phys. Rev. B **33**, 6821 (1986).
[30] For a recent review on CuPt-type ordering and CuAu-type ordering, see A. Zunger and S. Mahajan, in *Handbook of Semiconductors*, 2nd ed., edited by S. Mahajan (Elsevier, Amsterdam, in press), Vol. 3, and references therein.
[31] For a review on chalcopyrite ordering, see J. L. Shay and J. H. Wernick, *Ternary Chalcopyrite Semiconductor*, (Pergamon, New York, 1975).
[32] S.-H. Wei and A. Zunger, Phys. Rev. B **39**, 3279 (1989).
[33] S.-H. Wei and A. Zunger, Appl. Phys. Lett. **56**, 662 (1990).
[34] S.-H. Wei, D. B. Laks, and A. Zunger, Appl. Phys. Lett. **62**, 1937 (1993); D. B. Laks, S.-H. Wei, and A. Zunger Phys. Rev. B **69**, 3766 (1992).
[35] R. G. Alonso, A. Mascarenhas, G. S. Horner, K. A. Bertness, S. R. Kurtz, and J. M. Olson, Phys. Rev. B **48**, 11 833 (1993).
[36] T. Kanata, M. Nishimoto, H. Nakayama, and T. Nishino, Phys. Rev. B **45**, 6637 (1992).
[37] J. E. Bernard , S.-H. Wei, D. M. Wood, and A. Zunger, Appl. Phys. Lett **52**, 311 (1988).
[38] S. Gopalan, M. Cardona, and N. E. Christensen, Solid State Commun. **66**, 471 (1988).
[39] L. I. Schiff, *Quantum Mechanics*, 3rd ed. (McGraw-Hill, New York, 1968), pp. 209–210.
[40] J. E. Jaffe and A. Zunger, Phys. Rev. B **28**, 5822 (1983).
[41] D. J. Chadi, Phys. Rev. B **16**, 790 (1977).
[42] J. J. Hopfield, J. Phys. Chem. Solids **15**, 97 (1960).
[43] A. Zunger and D. M. Wood, J. Cryst. Growth **98**, 1 (1989).
[44] D. B. Laks, L. G. Ferreira, S. Froyen, and A. Zunger, Phys. Rev. B **46**, 12 587 (1992).
[45] *Numerical Data and Functional Relationships in Science and Technology*, edited by O. Madelung, M. Schulz, and H. Weiss, Landolt-Börnstein, New Series, Group III, Vol. 17a (Springer-Verlag, Berlin, 1982).
[46] S.-H. Wei and H. Krakauer, Phys. Rev. Lett. **55**, 1200 (1985), and references therein.
[47] P. Hohenberg and W. Kohn, Phys. Rev. **136**, B864 (1964); W. Kohn and L. J. Sham, *ibid.* **140**, A1133 (1965).
[48] D. M. Ceperly and B. J. Alder, Phys. Rev. Lett. **45**, 566 (1980); J. P. Perdew and A. Zunger, Phys. Rev. B **23**, 5048 (1981).
[49] D. Olego, M. Cardona, and H. Muller, Phys. Rev. B **22**, 894 (1980).
[50] J. L. Martins and A. Zunger, Phys. Rev. B **30**, 6217 (1984).
[51] The ratio λ is loosely related to the ionicity defined by J. C. Phillips, *Bonds and Bands in Semiconductors* (Academic, New York, 1973), p. 42. In general, as ionicity increases, λ decreases.
[52] L. Vegard, Z. Phys. **5**, 17 (1921).
[53] K. Mader and A. Zunger (unpublished).
[54] C. Bocchi, P. Franzosi, and C. Ghezzi, J. Appl. Phys. **57**, 4533 (1985).
[55] A. Compaan, R. C. Bowman, and D. E. Cooper, Semicond. Sci. Technol. **5**, 573 (1990).
[56] S. Perkowitz, L. S. Kim, and P. Becla, Phys. Rev. B **43**, 6598 (1991).
[57] K. Beshah, D. Zamir, and P. Becla, P. A. Wolff, and R. G.

Griffin, Phys. Rev. B **36**, 6420 (1987).
[58] D. T. Pierce and F. Meier, Phys. Rev. B **13**, 5484 (1976).
[59] T. Kanata, M. Nishimoto, H. Nakayama, and T. Nishino, Appl. Phys. Lett. **63**, 26 (1993).
[60] F. Alsina, J. Pascual, E. Massone, J. Camassel and J. P. Andre, Jpn. J. Appl. Phys. (to be published); F. Alsina, Ph.D. thesis, Universitat Autonoma de Barcelona, Spain, 1993.
[61] G. W. 't Hooft, C. J. B. Riviere, M. P. C. M. Krijn, C. T. H. F. Liedenbaum, and A. Valster, Appl. Phys. Lett. **61**, 3169 (1992).
[62] A. Mascarenhas, S. Kurtz, A. Kibbler, and J. M. Olson, Phys. Rev. Lett. **63**, 2108 (1989).
[63] F. Ciccacci, E. Molinari, and N. E. Christensen, Solid State Commun. **62**, 1 (1987).
[64] L. J. Sham, J. Phys. C **5**, A51 (1993).
[65] T. Omori *et al.*, Phys. Rev. Lett. **67**, 3294 (1991).